Journal of Biomechanics 179 (2025) 112485

Contents lists available at ScienceDirect

Journal of Biomechanics

journal homepage: www.elsevier.com/locate/jbiomech

Plaque heterogeneity influences in-stent restenosis following drug-eluting stent implantation: Insights from patient-specific multiscale modelling

Anna Corti [a,*], Lucia Dal Ferro [b,e,f], Ali C. Akyildiz [c,d], Francesco Migliavacca [b], Sean McGinty [e,f], Claudio Chiastra [g]

[a] Department of Electronics, Information and Bioengineering, Politecnico di Milano, Milan, Italy
[b] Laboratory of Biological Structure Mechanics (LaBS), Department of Chemistry, Materials and Chemical Engineering "Giulio Natta", Politecnico di Milano, Milan, Italy
[c] Department of Cardiology, Biomedical Engineering, Cardiovascular Institute, Thorax Center, Erasmus MC, Rotterdam, the Netherlands
[d] Department of Biomechanical Engineering, Delft University of Technology, Delft, the Netherlands
[e] Division of Biomedical Engineering, University of Glasgow, Glasgow, UK
[f] Glasgow Computational Engineering Centre, University of Glasgow, Glasgow, UK
[g] PoliTo^{BIO}Med Lab, Department of Mechanical and Aerospace Engineering, Politecnico di Torino, Turin, Italy

ARTICLE INFO

Keywords:
Agent-based model (ABM)
Drug transport model
Percutaneous coronary intervention
Coronary artery
Atherosclerotic plaque

ABSTRACT

In-stent restenosis represents a major cause of failure of percutaneous coronary intervention with drug-eluting stent implantation. Computational multiscale models have recently emerged as powerful tools for investigating the mechanobiological mechanisms underlying vascular adaptation processes during in-stent restenosis. However, to date, the interplay between intervention-induced inflammation, drug delivery and drug retention has been under-investigated.

Here, an original patient-specific multiscale agent-based modelling framework was developed to investigate the interplay between drug release, plaque composition and intervention-induced inflammation on in-stent restenosis following drug-eluting stent implantation. The framework integrated a finite element simulation of stent expansion, with a drug transport simulation and an agent-based model of cellular dynamics. A patient-specific coronary cross-section with heterogeneous diseased tissue was considered and rigorously analyzed through a variety of scenarios, including different plaque compositions and different inflammatory responses.

The analysis revealed three significant findings: (i) calcifications substantially impeded drug transport, resulting in drug-depleted regions and reduced stent efficacy; (ii) by impacting drug transport, variations in plaque composition influenced arterial wall response, with the fully-calcific scenario showing the greatest lumen area reduction; (iii) the impact of different drug receptor saturation conditions (obtained with different plaque compositions) was particularly evident under conditions of persistent inflammatory state.

This study represents a significant advancement in multiscale modelling of in-stent restenosis following drug-eluting stent implantation. The results obtained provided deeper insights into the complex interactions among patient-specific plaque composition, inflammation and drug retention, suggesting a patient-specific management of the intervention, particularly in cases of complex disease.

1. Introduction

With about 8.9 million annual deaths worldwide, coronary artery disease represents the leading cause of vascular morbidity and mortality (GBD 2017 Causes of Death Collaborators, 2018). Nowadays, percutaneous coronary intervention with drug-eluting stent implantation is the preferred endovascular treatment. However, the procedure still suffers from in-stent restenosis, which represents a major cause of intervention failure, with rates up to 10 % (Alfonso et al., 2022; Shlofmitz et al., 2019). In-stent restenosis is the result of the inflammatory-driven maladaptive response to the vascular injury and manifests as exacerbated synthetic smooth muscle cell (SMC) proliferation and extracellular matrix (ECM) deposition, leading to lumen re-narrowing after stent implantation (Aoki and Tanabe, 2021). Despite the ubiquitous use of drug-eluting stent, which have substantially reduced neointima hyperplasia and in-stent restenosis, optimal drug delivery strategies that prevent in-

* Corresponding author at: Department of Electronics, Information and Bioengineering, Politecnico di Milano, Via Ponzio 34/5, 20133 Milan, Italy.
E-mail address: anna.corti@polimi.it (A. Corti).

https://doi.org/10.1016/j.jbiomech.2024.112485
Accepted 15 December 2024
Available online 16 December 2024

stent restenosis remain elusive (McQueen et al., 2021). For this purpose, a deep understanding of the complex interplay between biological, mechanical, hemodynamic, drug release and procedural factors driving the arterial response to the intervention, and consequently potential in-stent restenosis, is essential (Aoki and Tanabe, 2021).

Recently, computational multiscale agent-based modeling frameworks that integrate continuous- and agent-based approaches have shown promise in describing the multiscale mechanobiological interplay of events underlying vascular adaptation processes such as in-stent restenosis (Corti et al., 2021; Nolan and Lally, 2018; Zahedmanesh et al., 2014; Zun et al., 2019, 2017). Generally, these frameworks combine a continuum-based description of the structural mechanics, hemodynamics, and/or transport mechanisms at the tissue level through numerical methods solving partial differential equations, with a discrete-based description of cellular behavior, cell–cell and cell-environment interactions at the cellular scale through an agent-based model (ABM). Although, several multiscale agent-based modeling frameworks have been proposed for studying in-stent restenosis (Corti et al., 2021), the interplay between drug kinetics and cellular dynamics has been under-investigated, with only a few studies implementing drug delivery through a simple diffusion-based model (Caiazzo et al., 2011; Tahir et al., 2013). Recently, Corti et al. (2023a) developed a multiscale agent-based modeling framework of in-stent restenosis following drug-eluting stent implantation, integrating a sophisticated drug model with binding kinetics at the continuum level and an ABM of cellular dynamics. As proof-of-concept study, different scenarios of drug mass, drug release profiles, coupling schemes (between the drug module and the ABM) and vessel cross-sectional geometries were explored, highlighting potential for optimizing drug-eluting stent design. However, the model output showed only a partial sensitivity to different scenarios, which was attributed to the under-investigated role of the inflammatory response and the neglect of arterial tissue heterogeneity. Indeed, only one abrupt and sharp inflammatory curve (which damped the effect of late drug release) was considered, although persistent and high levels of vascular inflammation were found to be associated with worse clinical outcomes (Kalkman et al., 2018). Moreover, uniform tissue layer properties were assumed, neglecting the impact of plaque composition on drug release, retention in tissue and, consequently, in-stent restenosis. The present study builds upon the previous one (Corti et al., 2023a) and aims to enhance understanding of the impact of drug release on in-stent restenosis by improving the multiscale agent-based modeling framework and proposing a novel investigation, through (i) the application of the framework to a patient-specific diseased coronary artery cross-section with heterogenous composition and different plaque materials, (ii) the inclusion of a stent implantation module, simulated through the finite element (FE) method, and (iii) the exploration of the effects of different plaque materials as well as different inflammatory responses on in-stent restenosis.

2. Methods

2.1. Multiscale framework

The multiscale in-stent restenosis framework takes a 2D diseased coronary artery cross-section and a post-intervention inflammatory curve as input, and generates the artery cross-section configuration at 1-month follow-up as output (Fig. 1). The framework consists of three modules: (i) the stent implantation module, (ii) the drug transport module and (iii) the tissue remodelling module. The stent implantation module receives the diseased coronary artery, performs a FE simulation of the Xience Prime drug-eluting stent (Abbott Laboratories, Abbott Park, IL, USA) expansion, and generates the deformed, stented artery geometry. The drug transport module simulates drug release and tissue retention along 1 month (McQueen et al., 2022), computing the receptor saturation, namely the local fraction of saturated target receptors over time. Finally, the tissue remodelling module simulates the 1-month post-intervention arterial wall remodelling due to the intervention-induced inflammation and the receptor saturation (passed from the drug transport module) through an ABM (Corti et al., 2023b, 2022b, 2022a). The spatial contour of receptor saturation is computed every 6 hours over 1 month and updated within the ABM. The 1-month follow-up was in line with the drug release profile of the Xience Prime drug-eluting stent (up to 75 % of drug released within the initial month) (Mukheja et al., 2024).

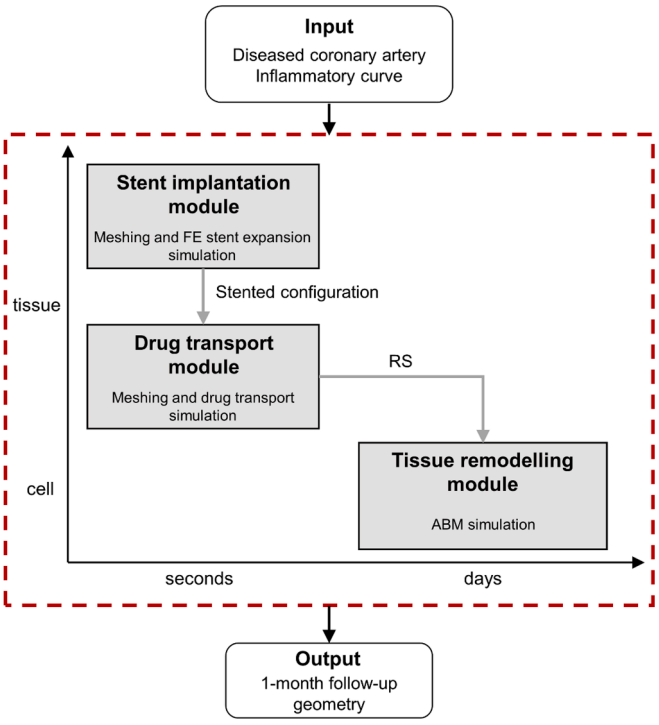

Fig. 1. Multiscale computational framework. Starting from the diseased coronary artery cross-section, the framework (dashed red box) simulates arterial wall remodelling and in-stent restenosis over 1-month of follow-up, generating as output the remodelled arterial geometry. The framework consists of three modules, namely (i) the stent implantation module at the tissue-second scale, in which the artery cross-section is meshed and the finite element (FE) simulation of stent expansion is performed to generate the stented configuration, (ii) the drug transport module at the tissue-seconds scale, in which the artery model is meshed and the drug transport simulation is performed to compute the receptor saturation (RS), and (iii) the tissue remodelling module at the cell-days scale, in which an agent-based model (ABM) simulates cellular activities and arterial wall remodelling in response to the intervention-induced inflammation and the RS, and generates the remodelled arterial configuration. (For interpretation of the references to colour in this figure legend, the reader is referred to the web version of this article.)

2.1.1. Stent implantation module

The patient-specific diseased coronary artery cross-section reported in Fig. 2 was considered. This cross-sectional geometry was reconstructed from post-mortem coronary artery data collected at the Erasmus Medical Center (Rotterdam, The Netherlands) (Guvenir Torun et al., 2021). The study was approved by the local Ethical Committee, and participants provided informed consent to participate in the study. Details on sample collection and geometry creation are provided in Guvenir Torun et al. (2021).

The coronary artery cross-section (Fig. 2A) had a lumen area of 4.08 mm^2, with minimum lumen diameter of 1.79 mm. It was characterized by a diseased two-layered arterial wall comprising a fibrous intimal layer, with two lipid pools and one calcification, and a media/adventitia layer (Guvenir Torun et al., 2021). The arterial wall was discretized using quadrilateral and triangular elements (CPE4R, CPE3). The tissue material properties previously calibrated through an inverse FE

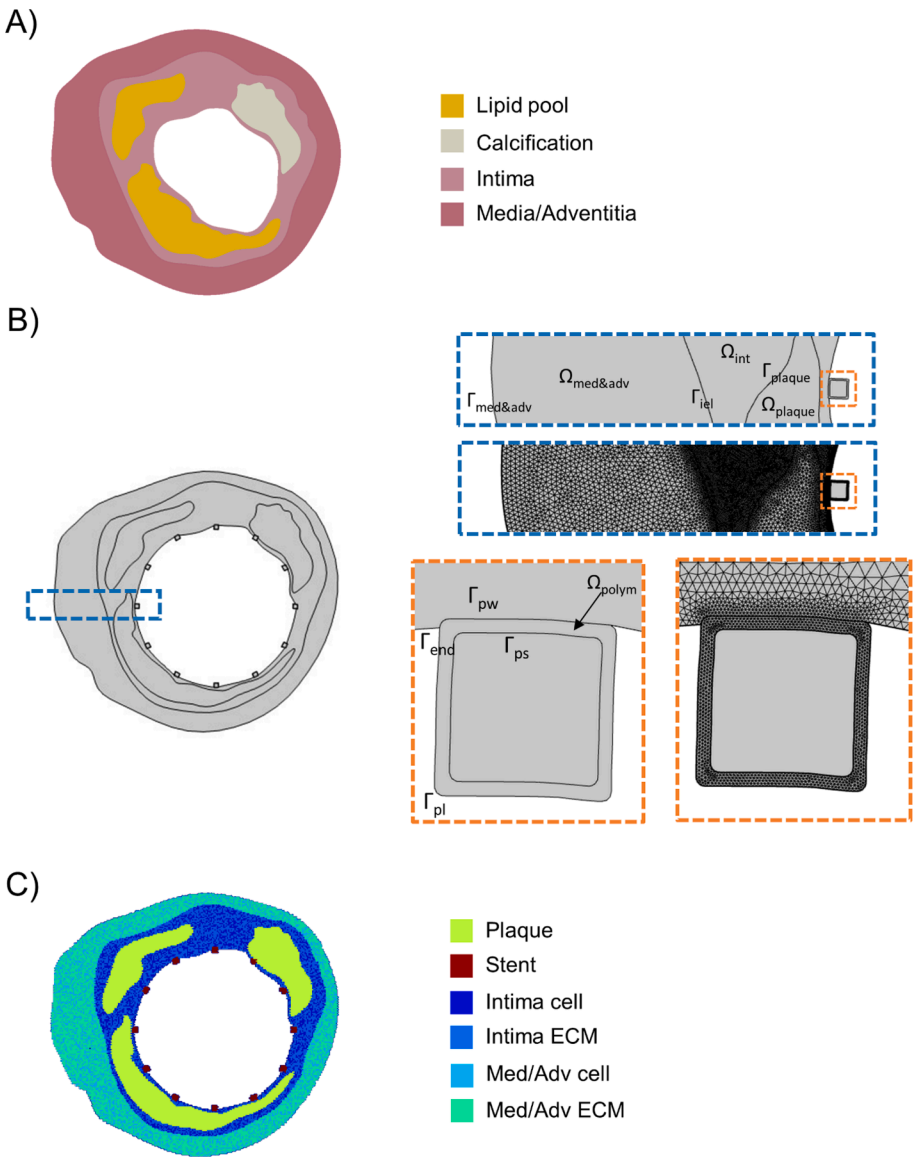

Fig. 2. A) Patient-specific diseased coronary artery cross-section; B) Drug transport model domains and mesh: stented coronary artery cross-section with schematic of the domains (Ω), boundaries (Γ) and geometric parameters, and representation of the finite element mesh on magnified portions of the geometry. C) Agent-based model of the patient-specific stented coronary artery cross-section.

modeling pipeline were used (Guvenir Torun et al., 2021). Specifically, the fibrous intima and media/adventitia layers were modelled as Yeoh materials, while the lipid and calcium components as Neo-Hookean materials, with material parameters provided in Table 1 (Gijsen et al., 2021; Guvenir Torun et al., 2021; Loree et al., 1994). All materials presented density of 1000 kg/m^3 and Poisson's ratio of 0.475 (assumed as quasi-incompressible (Milzi et al., 2021; Stefanati et al., 2024)). Additionally, the FE coronary artery model was surrounded by a circular external structure of 10 mm of diameter for the imposition of boundary conditions, modelled as a compressible Neo-Hookean material with material constant of 100 kPa, which practically reduced the rigid body motion of the artery structure and accounted for the perivascular compliant tissue. The Xience Prime drug-eluting stent (Abbott Laboratories, Abbott Park, IL, USA) was used, featuring 12 equally-spaced square struts of 81 μm thickness, with 8 μm thick polymer coating, and a nominal diameter of 3 mm. The stent material was modelled as linear elastic, with Young's Modulus of 243 GPa (Mandal et al., 2016).

The 2D FE simulation of stent expansion was performed in Abaqus/Explicit (Dassault Systemes, Simulia corp., USA), under plane strain assumption. The simulation consisted of three steps (Supplementary

Table 1
Mechanical properties of the arterial tissue components, from Guvenir Torun et al (2021).

	Fibrous intima	Arterial wall	Calcium	Lipid tissue
Constitutive model	$W_{Yeoh} = \sum_{i=1}^{3} c_i \bullet (I_1 - 3)^i$		$W_{Neo-Hookean} = c_1 \bullet (I_1 - 3)$	
c_1 [kPa]	18.99	0.42	1000	1
c_2 [kPa]	−96.68	0.59	–	–
c_3 [kPa]	289.37	21.60	–	–

Figure 1S): (i) a pressurization step, where a uniform intraluminal pressure of 100 mmHg was applied to the coronary artery luminal surface and maintained throughout the entire simulation, (ii) an inflation step, where the stent struts were radially expanded by applying a displacement condition up to a diameter of 3.1 mm to an internal circular surface representing the balloon, and (iii) a deflation step, in which the surface collapsed. The general contact algorithm, with a 'hard' normal behaviour and a tangential behaviour with friction coefficient of 0.2 was set to define the interaction between the struts and the lumen border of the coronary artery cross-section (Corti et al., 2022a). Nodes on the external surface of the surrounding structure were fixed (zero-displacement boundary condition).

Table 2
Drug transport model equations.

Polymer (Ω_p)	$\frac{\partial c_p}{\partial t} = D_p \nabla^2 c_p,\ c_p(t=0) = c_p^0 = \frac{M^0}{V_p}$
Intima (Ω_i)	$\boldsymbol{u}_i = -\frac{K_i}{\mu_p}\nabla p_i, \nabla \bullet \boldsymbol{u}_i = 0$
	$\frac{\partial c_i}{\partial t} + \frac{\gamma_i}{\phi_i}\boldsymbol{u}_i \bullet \nabla c_i = \nabla \bullet (\boldsymbol{D}_i \nabla c_i) - \frac{\partial b^s}{\partial t} - \frac{\partial b^{ns}}{\partial t},\ c_i(t=0) = 0$
	$\frac{\partial b^s}{\partial t} = k_{on}^s c_i \left(b_{max}^s - b^s\right) - k_{off}^s b^s,\ b^s(t=0) = 0$
	$\frac{\partial b^{ns}}{\partial t} = k_{on}^{ns} c_i \left(b_{max}^{ns} - b^{ns}\right) - k_{off}^{ns} b^{ns},\ b^{ns}(t=0) = 0$
	$RS_{map} = \frac{b^s}{b_{max}^s};\ RS_{curve} = \frac{1}{V_i}\int_{Vi} \frac{b^s}{b_{max}^s} dV_w$
Lipid (Ω_l)	$\boldsymbol{u}_l = -\frac{K_l}{\mu_p}\nabla p_l, \nabla \bullet \boldsymbol{u}_l = 0$
	$\frac{\partial c_l}{\partial t} + \frac{\gamma_l}{\phi_l}\boldsymbol{u}_l \bullet \nabla c_l = \nabla \bullet (\boldsymbol{D}_l \nabla c_l) - \frac{\partial b^s}{\partial t} - \frac{\partial b^{ns}}{\partial t},\ c_l(t=0) = 0$
	$\frac{\partial b^{ns}}{\partial t} = k_{on}^{ns} c_l \left(b_{max}^{ns} - b^{ns}\right) - k_{off}^{ns} b^{ns},\ b^{ns}(t=0) = 0$
Media/Adventitia (Ω_{ma})	$\boldsymbol{u}_{ma} = -\frac{K_{ma}}{\mu_p}\nabla p_{ma}, \nabla \bullet \boldsymbol{u}_{ma} = 0$
	$\frac{\partial c_{ma}}{\partial t} + \frac{\gamma_{ma}}{\phi_{ma}}\boldsymbol{u}_{ma} \bullet \nabla c_{ma} = \nabla \bullet (\boldsymbol{D}_{ma} \nabla c_{ma}),\ c_{ma}(t=0) = 0$
	$\frac{\partial b^{ns}}{\partial t} = k_{on}^{ns} c_{ma} \left(b_{max}^{ns} - b^{ns}\right) - k_{off}^{ns} b^{ns},\ b^{ns}(t=0) = 0$

c_p: drug concentration in the polymer; D_p: effective polymer coating diffusion coefficient; c_p^0: initial drug concentration in the polymer; M^0: initial mass of drug; V_p: volume of the coating per strut; $\boldsymbol{u}_i$: transmural velocity in the intima; K_i: Darcy permeability in the intima; μ_p: plasma dynamic viscosity; p_i: pressure field in the intima; c_i: dissolved drug concentration in the intima; γ_i: hindrance coefficient in the intima; ϕ_i: intima porosity; $\boldsymbol{D_i}$: diffusivity tensor of the intima; b^s: concentration of specifically bound drug; k_{on}^s: specific binding on rate; k_{off}^s: specific binding off rate; b_{max}^s: specific binding site maximum density; b^{ns}: concentration of non-specifically bound drug; k_{on}^{ns}: non-specific binding on rate; k_{off}^{ns}: non-specific binding off rate; b_{max}^{ns}: non-specific binding site maximum density; RS_{map}: spatial contour of receptor saturation (RS) at a specific time instant; RS_{curve}: time-varying mean RS over space; V_i: intima volume; $\boldsymbol{u_l}$: transmural velocity in the lipid; K_l: Darcy permeability in the lipid; p_l: pressure field in the lipid; c_l: dissolved drug concentration in the lipid; γ_l: hindrance coefficient in the lipid; ϕ_l: lipid porosity; $\boldsymbol{D_l}$: diffusivity tensor of the lipid; $\boldsymbol{u}_{ma}$: transmural velocity in the media/adventitia; K_{ma}: Darcy permeability in the media/adventitia; p_{ma}: pressure field in the media/adventitia; c_{ma}: dissolved drug concentration in the media/adventitia; γ_{ma}: hindrance coefficient in the media/adventitia; ϕ_{ma}: media/adventitia porosity; $\boldsymbol{D_{ma}}$: diffusivity tensor of the media/adventitia. The values and references of all the parameters are provided in Supplementary Table 1S.

2.1.2. Drug transport module

The drug transport module was adapted from Corti et al. (2023a) to account for heterogeneous arterial tissue composition. A FE mesh of triangular elements was created in COMSOL Multiphysics (COMSOL AB, Burlington, MA, USA) (Fig. 2B). Transient simulations of Sirolimus drug transport were performed in COMSOL Multiphysics (Escuer et al., 2022, 2021; McQueen et al., 2022), implementing: (i) drug release from a durable coating, modelled as a diffusion process (McGinty, 2014), (ii) drug transport within the porous arterial tissues, modelled by coupling Darcy's law with advection–diffusion-reaction equations, and (iii) drug retention, modelled with nonlinear saturable binding kinetics, by applying specific-binding (b^s) to cells in the fibrous intima and non-specific binding (b^{ns}) to non-cellular components in all the arterial tissues. The calcification was considered as a non-diffusive, non-permeable, and non-porous region (Escuer et al., 2022). Moreover, while non-specific binding kinetics were modelled in the intima, lipid and media/adventitia tissues, specific binding kinetics were modelled only in the intima. The drug transport model equations are provided in Table 2, with parameter values and references detailed in Supplementary Table 1S, and boundary conditions in Table 3. Receptor saturation was computed at each time step over the domain and the spatial contour was exported every 6 simulated hours as RS_{map}.

2.1.3. Tissue remodelling module

The tissue remodelling module consisted of the 2D ABM simulation of arterial wall remodelling in response to the intervention-induced inflammation and released drug (Corti et al., 2023a). Fig. 2C shows the ABM of the two-layer stented coronary artery cross-sections, composed of intima, plaques and media/adventitia layers. Briefly, the ABM was generated on a 300 × 300 hexagonal grid by scaling the nodal coordinates obtained from the drug transport module by a 25 μm/ABM site scale factor (SMC diameter of 25 μm (Tahir et al., 2015)). Cells and ECM composed the intima and media/adventitia layers, with specific densities (Corti et al., 2024, 2023b, 2022a, 2022b; Serafini et al., 2023). An inflammatory curve (I), representing the time-varying post-intervention inflammatory response along 1 month, and the RS_{map}, representing the local and instantaneous fraction of SMCs bound to drug (updated every 6 simulated hours), were used to initialize the ABM and drive cellular activities. Probabilistic rules were defined to simulate cellular mitosis/apoptosis and ECM production/degradation in response to I and RS_{map} in the intima, and homeostatic activities in the adventitia as detailed in Table 4 (Corti et al., 2023a). Specifically, in the intima layer, the inflammatory response I determines an increase in the proliferative and synthetic cellular activities ($p_{division}^h$ and $p_{ECMproduction}^h$), while receptor saturation determines a reduction of cellular mitosis, due to the cytostatic effect of drug ($p_{division}^h$). In the media/adventitia layer, or in the intima layer in case of absence of stimuli, baseline activities are set to ensure a balance of cellular mitosis and apoptosis, and of ECM production and degradation. The parameters were defined according to

Table 3
Drug transport model boundary conditions.

Boundary	Condition
Polymer coating-strut interface (Γ_{ps})	Zero-flux (Bozsak et al., 2014)
Polymer coating-lumen interface (Γ_{pl})	Infinite sink (Bozsak et al., 2014)
Endothelium (Γ_{et})	Infinite sink (Escuer et al., 2022)
Polymer coating-wall interface (Γ_{pw})	Continuity (Bozsak et al., 2014; Escuer et al., 2022)
Internal elastic lamina (IEL) (Γ_{iel})	Kedem-Katchalsky (Escuer et al., 2022)
Perivascular edge (Γ_{adv})	Infinite sink (Bozsak et al., 2014; Escuer et al., 2022)
Intima-Lipid regions	Kedem-Katchalsky (Colombo et al., 2021)
Intima-Calcium region	Zero-flux (Gijsen et al., 2021)

Table 4
Agent-based model probability equations.

Intima	$p^h_{division} = (\alpha_1 + \alpha_2 I^h)(1 - \alpha_3 RS_{ABM}{}^h)$
	$p^h_{apoptosis} = \alpha_1$
	$p^h_{ECMproduction} = \alpha_4 + \alpha_5 I^h$
	$p^h_{ECMdegradation} = \frac{\alpha_4}{\beta_{int}}$
Media/Adventitia	$p^h_{division} = p^h_{apoptosis} = \alpha_1$
	$p^h_{ECMproduction} = \beta_{med/adv} \bullet p^h_{ECMdegradation} = \alpha_4$
Parameters	$\alpha_1 = 0.0025$; $\alpha_2 = 0.05$; $\alpha_3 = 1$; $\alpha_4 = 0.0004$; $\alpha_5 = 0.0125$
	βint = 1.55; βmed/adv = 2.5

$p^h_{division}$: probability of cell mitosis; $p^h_{apoptosis}$: probability of cell apoptosis; $p^h_{ECMproduction}$: probability of extracellular matrix (ECM) production; $p^h_{ECMdegradation}$: probability of ECM degradation; I: inflammatory input; RS_{ABM}: receptor saturation input; α_1, α_2, α_3, α_4, α_5, β_{med}, β_{adv}: parameters driving agent probabilities.

Corti et al. (2023a). Comprehensive details on the definition of probabilistic rules can be found in previous studies (Corti et al., 2024, 2023b, 2022a, 2022b).

The ABM simulation involves executing agent activities at each 2-hour time step. To desynchronize cellular activities, each agent is initialized with a random time within its biological cycle T_{agent} (T_{cell} = 24 h and T_{ECM} = 4 h), which is updated at each time step. When agents reach the end of their biological cycle, they become potentially active, and their internal time is reset at the following step. Accordingly, at each time step, potentially active agents are identified, and the manifestation of the agent-specific event (cell mitosis/apoptosis or ECM production/degradation) is tested: the event occurs only if the agent-specific event probability exceeds a randomly generated number. An agent is generated in the case of cell mitosis and ECM production, while it is removed in the case of cell apoptosis and ECM degradation. Agent generation/removal within the arterial wall is inward-oriented in the intima, thus associated to a lumen area change, and outward-oriented in the media/adventitia, thus not affecting the lumen area. Finally, smoothing algorithms are applied to maintain regular contours (Corti et al., 2023b, 2022b, 2022a).

To account for the ABM stochasticity, the simulation was repeated three times, and the one with the output minimizing the root mean square deviation of the lumen contour from the average one was selected as the representative condition, and shown.

2.2. Investigated scenarios

To explore the impact of tissue heterogeneity and different plaque composition on drug release and subsequent remodelling processes, three coronary material configurations were considered, by maintaining the same stented vessel geometry and varying the plaque components: the original case (O), presenting two lipid pools and one calcification; the fully-lipidic case (L), presenting all lipid pools; and the fully-calcific case (C), presenting all calcifications (Fig. 3A). The drug transport module was run by modifying the assignment of the lipid and calcium transport properties to the different plaque regions, resulting in different receptor saturation maps for the three (O, L and C) cases.

Additionally, three inflammatory curves were generated to investigate the relative interplay between inflammatory state and drug retention on cellular activation and subsequent arterial wall response. Fig. 3B depicts the three inflammatory curves, which represent potential scenarios characterized by varying degrees and persistence of vascular

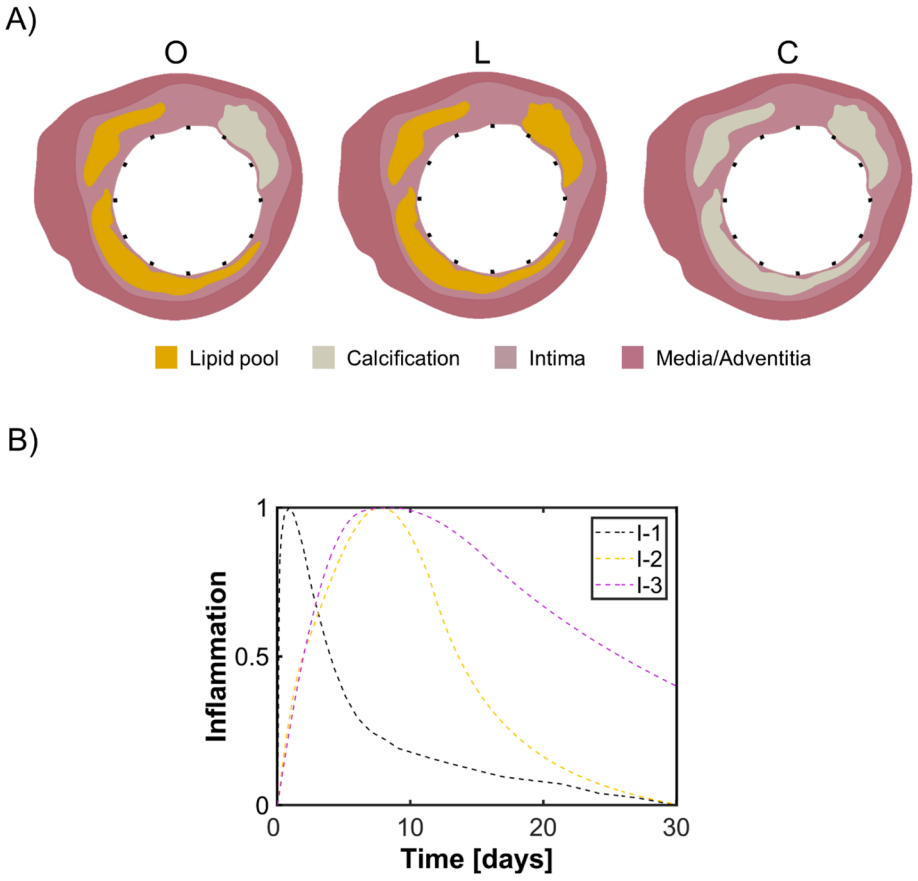

Fig. 3. Investigated plaque composition (A) and inflammatory scenarios (B). Each of the plaque composition case (O: original, L: fully-lipidic and C: fully-calcific) was considered in combination with each of the inflammatory input.

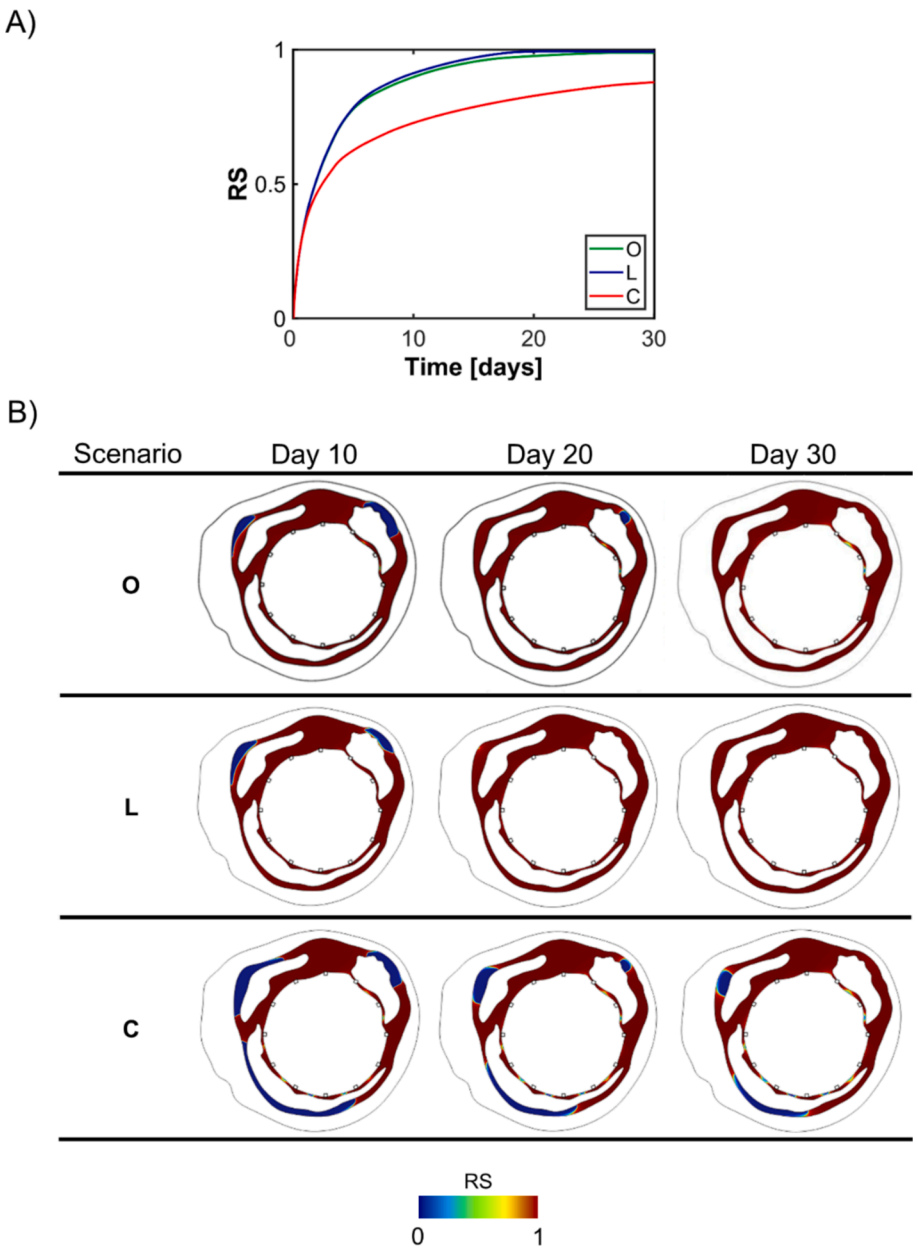

Fig. 4. Receptor saturation curves (A) and contour maps (B) for the different plaque composition scenarios (O: original, L: fully-lipidic, C: fully-calcific).

inflammation that may realistically arise following percutaneous coronary intervention (Edelman and Rogers, 1998; Kalkman et al., 2018; Schillinger et al., 2002a, 2002b): I-1 (previously used in (Corti et al., 2023a)), presenting a sharp peak around day 1 and an abrupt decay, with most of the inflammatory response occurring within 5 post-operative days and completely resolving within 1 month; I-2, presenting a peak around day 8 and a smooth decay, with most of the inflammatory response occurring within 20 days and completely resolving within 1 month; and I-3, presenting a peak around day 12 and a very smooth decay with a residual 30 % inflammatory state at 1 month. The rationale for the formulation of the three inflammatory curves is detailed in the Supplementary Material.

3. Results

Fig. 4 shows the receptor saturation curves and contours over 1 post-operative month obtained by the drug transport module considering the three plaque composition scenarios (O, L, and C). Case L resulted in similar receptor saturation as case O; the only difference between these cases is that one of the three plaque components has different properties. While negligible differences were observed in terms of receptor saturation curve over time (i.e., spatial-averaged receptor saturation), the spatial contour of receptor saturation reflected the impact of the calcification, which acted as a barrier to the transport of drug (Fig. 4). Consequently, a drug-depleted zone emerged behind the calcification up to day 20 in case O (Fig. 4B). The effect of calcifications was even more evident in case C, which resulted in a significantly different receptor saturation compared to cases O and L, both in terms of average trend and spatial contour over time (Fig. 4). Indeed, when all the plaque regions were modelled as calcific, less effective transport of drug was obtained, with the presence of large drug-depleted zones behind all the plaque regions (Fig. 4B). Even after 30 days, large areas exhibited very low drug concentrations, increasing the probability of cellular proliferation, contributing to in-stent restenosis. Overall, these results highlighted the impact of plaque composition on drug release, with lipid pools favouring the transport of drug, and consequently drug retention, compared to

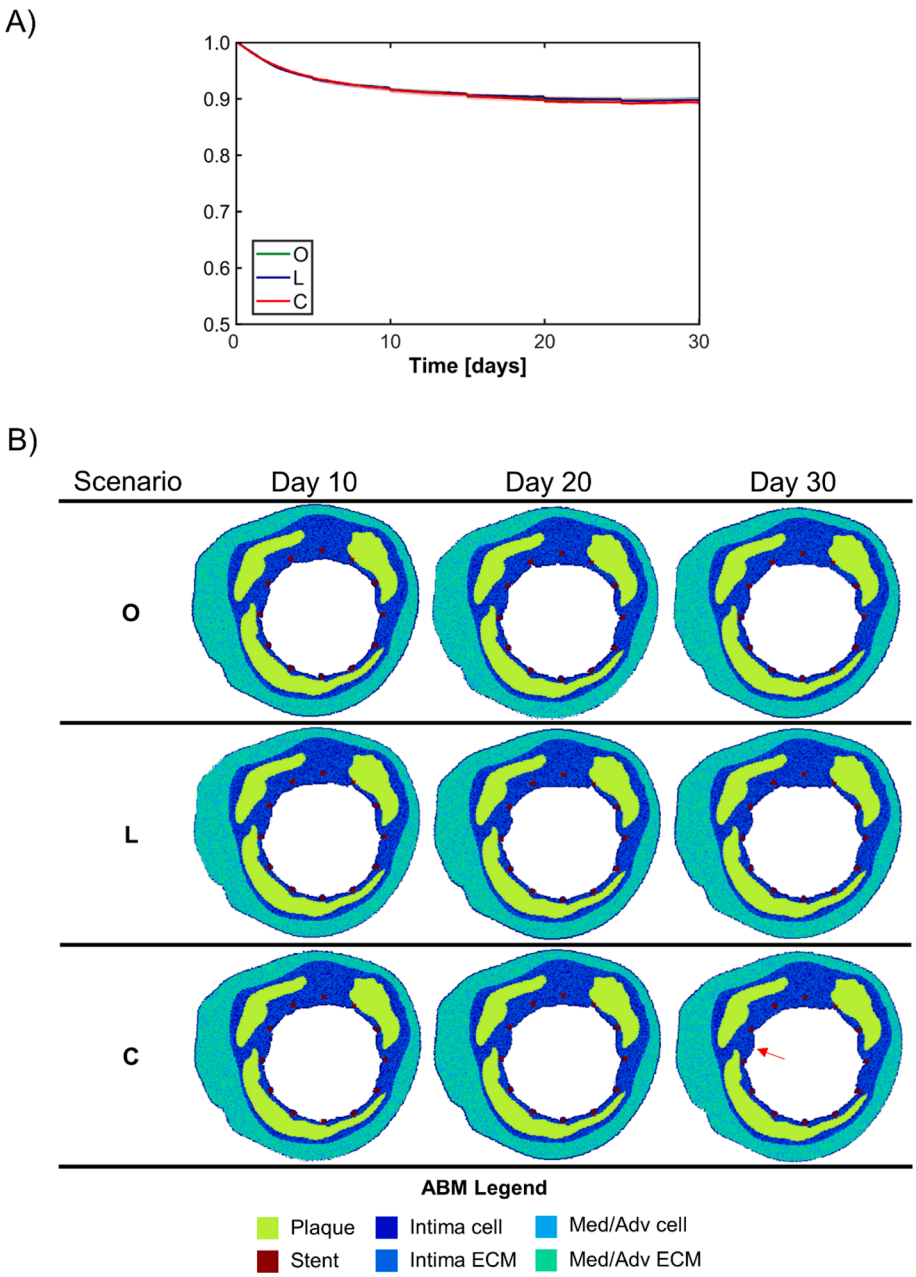

Fig. 5. Results of the tissue remodeling module in response to the inflammatory curve I-1 for the different plaque composition scenarios (O: original, L: fully-lipidic, C: fully-calcific). A) Normalized lumen area over time; B) Temporal evolution of the agent-based model (ABM) for the O, L and C scenarios: for each ABM plane, the results were retrieved from one out of three ABM simulations, namely the one presenting the lumen configuration minimizing the root mean square deviation from the average one.

calcific plaques.

Figs. 5, 6 and 7 show the arterial wall remodelling over 1-month follow-up in response to the different receptor saturation (obtained from cases O, L and C), for the three inflammatory curves (I-1, I-2 and I-3), respectively. It is evident that the arterial remodelling is affected by the interplay between receptor saturation and the inflammatory input. Particularly, when considering I-1, a constant 10 % lumen area reduction over 1 month was observed across all cases, irrespective of plaque composition (Fig. 5A). Minor local morphological variations in intimal growth patterns were detected, as indicated by the red arrow in Fig. 5B. The slightly larger local growth obtained in case C (red arrow, Fig. 5B) compared to cases O and L reflected the presence of the larger drug-depleted zones nearby. As the inflammatory stimulus persisted longer (i.e., I-2 and I-3), the lumen area reduction increased in all cases (O, L and C) and the impact of plaque composition became more pronounced. Particularly, with I-2, a 1-month lumen area reduction of 19 %, 19 % and 21 % was observed in cases O, L and C, respectively (Fig. 6A), increasing to 33 %, 33 % and 38 % with I-3 (Fig. 7A). In both cases, localized higher intimal growth was observed in case C near the drug-depletion zones, highlighting the role of calcifications in hindering effective drug transport (Fig. 6B and 7B). Finally, while a stabilization of the lumen area at 1-month was noted in response to I-1 and I-2 (Fig. 5A and 6A), a plateau was not reached with I-3 (Fig. 7A), suggesting that longer follow-up times would reveal further reductions in lumen area.

4. Discussion

In this work, a patient-specific multiscale agent-based modelling

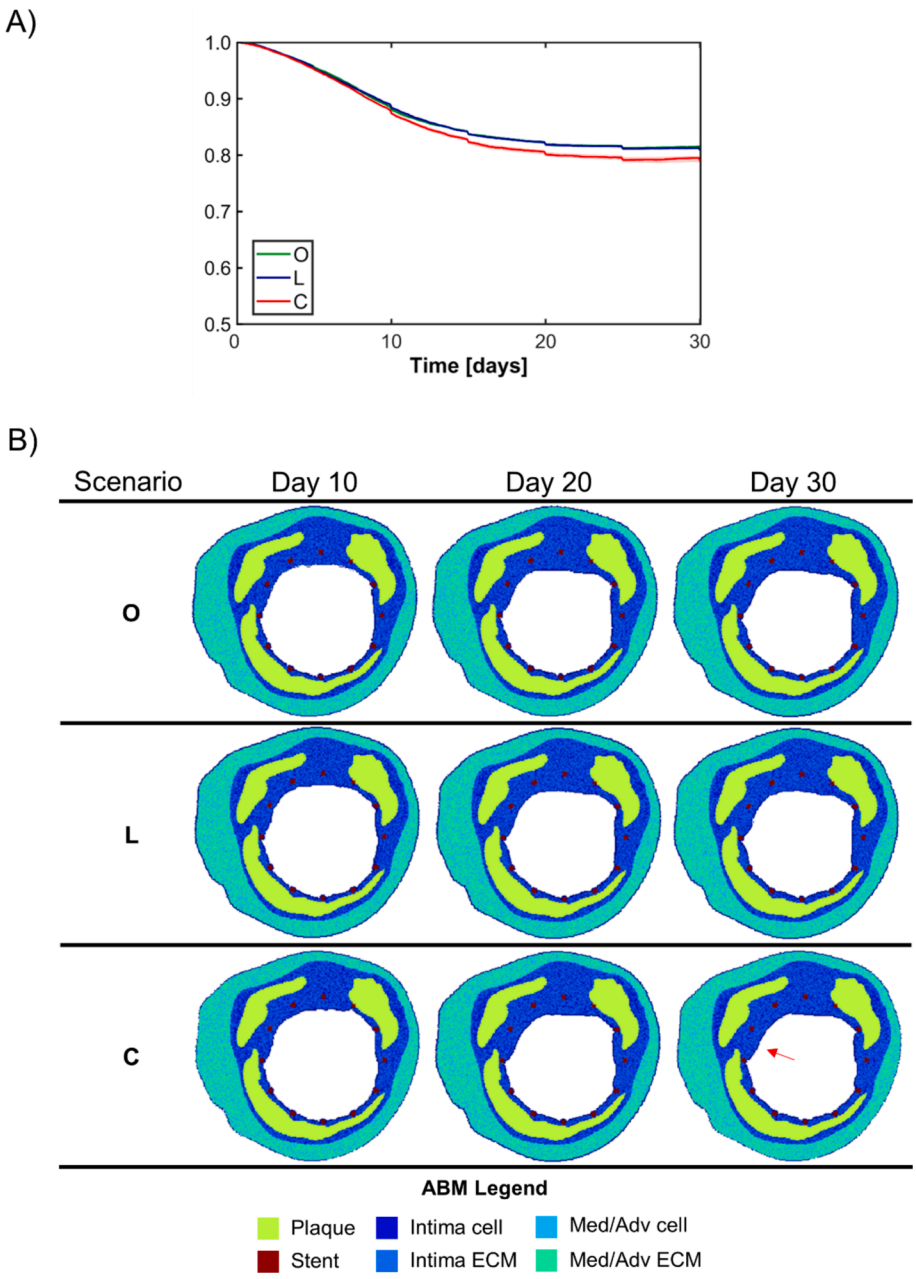

Fig. 6. Results of the tissue remodeling module in response to the inflammatory curve I-2 for the different plaque composition scenarios (O: original, L: fully-lipidic, C: fully-calcific). A) Normalized lumen area over time; B) Temporal evolution of the agent-based model (ABM) for the O, L and C scenarios: for each ABM plane, the results were retrieved from one out of three ABM simulations, namely the one presenting the lumen configuration minimizing the root mean square deviation from the average one.

framework was developed to investigate the interplay between drug release, plaque composition and intervention-induced inflammation on in-stent restenosis following drug-eluting stent implantation. The study introduced significant advancements to the previous work proposed by the authors and addressed the major limitations that were previously encountered (Corti et al., 2023a). First, a patient-specific diseased coronary cross-section was considered, thus accounting for heterogeneous arterial wall tissue, with lipid pools and calcifications. Second, the framework was enriched with a stent implantation module, enabling the generation of a realistic stented geometry from the diseased coronary artery cross-section. Third, the impact of different plaque compositions on the drug transport and on the subsequent arterial wall response was explored. Finally, the effect of different inflammatory conditions, accounting for possible diverse intervention-induced insults, was investigated.

Specifically, applying the multiscale framework to a patient-specific diseased coronary cross-section represents the primary innovation, marking substantial advancement in the in-silico modelling of in-stent restenosis development. The drug transport model was modified to include tissue-specific transport properties, providing deeper insights into how different plaque compositions affect drug release, stent efficacy, and resultant in-stent restenosis. This analysis was deepened by simulating two additional scenarios, namely a fully lipidic and a fully calcific plaque, achieved by adjusting the transport properties of the plaque regions. Moreover, by investigating the combinations of the three plaque composition scenarios (the original one, with mixed plaques, the fully-lipidic one and the fully-calcific one), with three post-intervention inflammatory curves, the following findings emerged: (i)

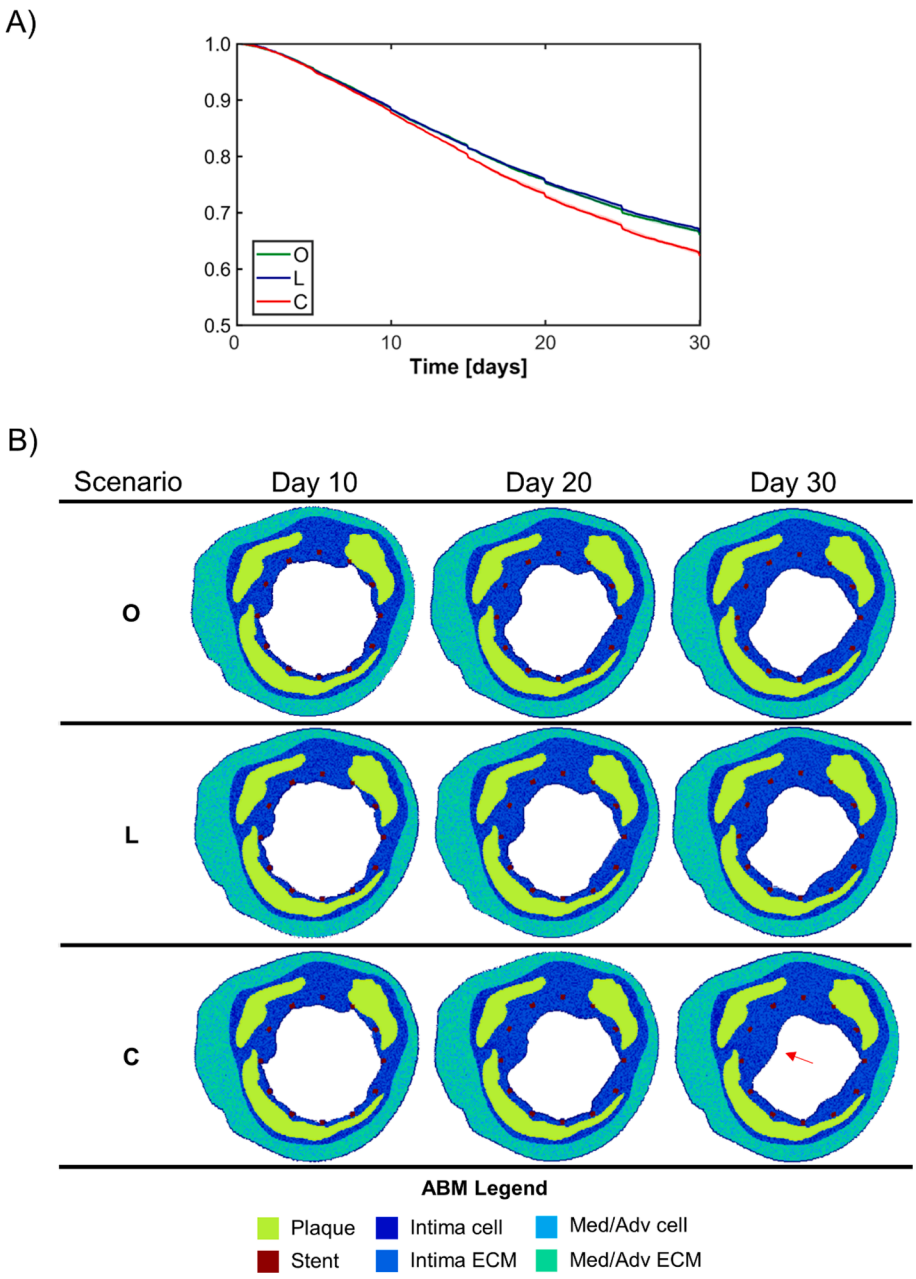

Fig. 7. Results of the tissue remodeling module in response to the inflammatory curve I-3 for the different plaque composition scenarios (O: original, L: fully-lipidic, C: fully-calcific). A) Normalized lumen area over time; B) Temporal evolution of the agent-based model (ABM) for the O, L and C scenarios: for each ABM plane, the results were retrieved from one out of three ABM simulations, namely the one presenting the lumen configuration minimizing the root mean square deviation from the average one.

calcifications substantially impeded drug transport, resulting in drug-depleted regions, and reduced stent efficacy; (ii) by having an impact on the drug transport, variations in plaque composition influenced arterial wall response, with the fully-calcific scenario showing the greatest lumen area reduction; (iii) the impact of different receptor saturation conditions (obtained with different plaque compositions) was particularly evident under conditions of persistent inflammatory state.

To the best of the authors' knowledge, this study represents the most sophisticated multiscale model of in-stent restenosis that accounts for the effect of drug release by the stent, as it integrates FE simulation of stent implantation, with a drug transport model incorporating tissue-specific transport properties and state-of-the-art binding kinetics, and an ABM of cellular dynamics responsive to both drug and inflammatory inputs. Besides the authors' previous investigation (Corti et al., 2023a), only two studies explored the effect of drug transport through ABMs of in-stent restenosis (Caiazzo et al., 2011; Tahir et al., 2011). However, these studies considered solely steady diffusion of free drug without incorporating binding kinetics and idealized vessel geometries with uniform tissue. Also at the continuum level, in-stent restenosis models including drug transport have been restricted to idealized geometries (McQueen et al., 2022). A recent study by Sarifuddin and Mandal (2024) investigated the impact of different plaque compositions on drug transport and retention, focusing on drug-coated balloons instead of drug-eluting stent. Similar to our work, they considered a patient-specific atherosclerotic arterial cross-section presenting with a heterogeneous tissue composition (healthy tissue, fibrous tissue, fibrofatty tissue, dense calcium and necrotic core), and generated "hard" and "soft" plaque alternative scenarios by modifying the tissue properties of

the fibrous and fibrofatty regions into calcium and necrotic core, and vice-versa, respectively. Although they considered a drug-coated balloon instead of a drug-eluting stent, their results on drug release and retention were consistent with ours. They observed a marked difference in the concentration of bound drug over time and in space between the "hard" model and the "soft"/original one, with the "hard" model showing lower concentrations compared to the others. It is important to note that the study by Sarifuddin and Mandal (2024) focused only on drug transport modelling and did not include arterial wall remodelling. Differently from their study, we were able to quantify how plaque-induced differences in drug transport affect neointima hyperplasia and eventually in-stent restenosis.

While this study presents significant advancements in modelling in-stent restenosis after drug-eluting stent implantation, it has limitations. These primarily arise from the decision to simplify the framework to focus specifically on drug release, retention, and the associated cellular responses under varying plaque compositions and inflammatory conditions. Accordingly, a simplified stent implantation module was implemented, achieving the primary aim of obtaining a stented configuration as initial state for the drug transport and tissue remodelling modules. Future studies could incorporate more sophisticated FE simulations of stent expansion to capture arterial wall stresses, strains or damage, which can be used as inputs for cellular dynamics in the ABM, as previously demonstrated (Corti et al., 2024, 2022a). Additionally, a spatially uniform, time-varying inflammatory curve was considered as the only restenosis trigger. This allowed us to focus on assessing the impact of diverse plaque composition on drug transport and subsequent in-stent restenosis without introducing confounding effects. Following the availability of patient-specific circulating inflammatory biomarkers (as gene expression or C-reactive protein data) personalized inflammatory profiles can be implemented, as done in our previous studies (Corti et al., 2023b, 2022b). Furthermore, to reflect the localized increase in inflammatory response in damaged regions, systemic inflammatory profiles can be adjusted locally based on intervention-induced trauma, as previously proposed (Corti et al., 2024). Moreover, since the framework is modular, various restenosis triggers, such as the above-mentioned structural stresses, strains or damage, or hemodynamic-based drivers (if a hemodynamic module is included), can be incorporated, as explored in previous works (Corti et al., 2024, 2023b, 2022a, 2022b; Nolan and Lally, 2018; Zahedmanesh et al., 2014; Zun et al., 2019, 2017). Additionally, the study was limited to a single 2D vessel geometry. Application of the model to several cross-sections or patients is needed to strengthen the results. Upon availability of patient-specific 3D coronary artery geometries with detailed tissue composition, our previously developed 3D-2D approach (Corti et al., 2023b, 2022b, 2022a) can be applied solving the stent implantation and drug transport modules in the 3D vessel geometry, and the tissue remodelling module at selected stented vessel cross-sections. Furthermore, here, a 1-month follow-up period was considered, being consistent with the typical drug release profile of the Xience Prime drug-eluting stent. However, longer follow-up times can be simulated. Finally, a limitation of the study lies in the lack of calibration and validation. Once longitudinal follow-up data become available, the framework can be calibrated and validated, leveraging established pipelines previously proposed, consisting of: (i) performing a sensitivity analysis on the ABM and drug transport parameters to identify the driving parameters, (ii) calibrating the identified parameters through the combination of surrogate modelling and genetic algorithm optimization, and (iii) applying the calibrated framework to different patient cases for validation (Corti et al., 2023b, 2022b).

Overall, this study represents a step forward in multiscale modelling of in-stent restenosis following drug-eluting stent implantation, by intentionally limiting the complexity to focus on the specific interactions between drug release, plaque composition, inflammation, and restenosis. In the future, a comprehensive 4-module framework, comprising stent implantation, drug transport, hemodynamics and tissue remodelling modules can be implemented, building on insights from our previous research.

5. Conclusions

The present study introduced a novel multiscale framework for investigating in-stent restenosis following drug-eluting stent implantation, integrating a stent implantation module with plaque composition-specific drug kinetics and an ABM of arterial wall remodelling. Applied to a patient-specific coronary artery cross-section with heterogeneous diseased tissue and considering different inflammatory triggers, our analysis provided deeper insights into the complex interactions among plaque composition, drug release and retention, inflammation and subsequent cellular response. While confined to a single vessel cross-section, the results highlighted that in-stent restenosis following drug-eluting stent implantation is likely to be impacted by the underlying plaque composition. Specifically, a coronary artery with calcifications exhibits lower concentrations of saturated receptors, resulting in reduced drug efficacy and potentially higher in-stent restenosis development. Moreover, the results underlined that the degree of in-stent restenosis also depends on the intensity and persistence of the pro-restenosis triggers. Future calibration and validation of the proposed multiscale framework model will allow obtaining a patient-specific predictive model of in-stent restenosis.

Data accessibility

All data supporting this study are provided within the main text and supplementary data.

CRediT authorship contribution statement

Anna Corti: Writing – review & editing, Writing – original draft, Visualization, Validation, Software, Methodology, Investigation, Formal analysis, Conceptualization. **Lucia Dal Ferro:** Writing – review & editing, Software, Methodology. **Ali C. Akyildiz:** Writing – review & editing, Data curation. **Francesco Migliavacca:** Writing – review & editing, Resources. **Sean McGinty:** Writing – review & editing, Supervision, Methodology, Conceptualization. **Claudio Chiastra:** Writing – review & editing, Supervision, Conceptualization, Methodology.

Declaration of competing interest

The authors declare that they have no known competing financial interests or personal relationships that could have appeared to influence the work reported in this paper.

Acknowledgements

AC is funded by the National Plan for NRRP Complementary Investments (PNC, established with the decree-law 6 May 2021, n. 59, converted by law n. 101 of 2021) in the call for the funding of research initiatives for technologies and innovative trajectories in the health and care sectors (Directorial Decree n. 931 of 06-06-2022) - project n. PNC0000003 - AdvaNced Technologies for Human-centrEd Medicine (project acronym: ANTHEM). This work reflects only the authors' views and opinions, neither the Ministry for University and Research nor the European Commission can be considered responsible for them.

SM and FM acknowledge funding provided by EPSRC (grant number EP/S030875/1). SM and CC acknowledge funding provided by EPSRC (grant number EP/Z531182/1).

Appendix A. Supplementary data

Supplementary data to this article can be found online at https://doi.org/10.1016/j.jbiomech.2024.112485.

References

Alfonso, F., Coughlan, J.J., Giacoppo, D., Kastrati, A., Byrne, R.A., 2022. Management of in-stent restenosis. EuroIntervention J. Eur. Collab. with Work. Gr. Interv. Cardiol. Eur. Soc. Cardiol. 18, e103–e123. https://doi.org/10.4244/EIJ-D-21-01034.

Aoki, J., Tanabe, K., 2021. Mechanisms of drug-eluting stent restenosis. Cardiovasc. Interv. Ther. 36, 23–29. https://doi.org/10.1007/s12928-020-00734-7.

Bozsak, F., Chomaz, J.-M., Barakat, A.I., 2014. Modeling the transport of drugs eluted from stents: physical phenomena driving drug distribution in the arterial wall. Biomech. Model. Mechanobiol. 13, 327–347. https://doi.org/10.1007/s10237-013-0546-4.

Caiazzo, A., Evans, D., Falcone, J.L., Hegewald, J., Lorenz, E., Stahl, B., Wang, D., Bernsdorf, J., Chopard, B., Gunn, J., Hose, R., Krafczyk, M., Lawford, P., Smallwood, R., Walker, D., Hoekstra, A., 2011. A Complex automata approach for in-stent restenosis: two-dimensional multiscale modelling and simulations. J. Comput. Sci. 2, 9–17. https://doi.org/10.1016/j.jocs.2010.09.002.

Colombo, M., Corti, A., Berceli, S., Migliavacca, F., McGinty, S., Chiastra, C., 2021. 3D modelling of drug-coated balloons for the treatment of calcified superficial femoral arteries. PLoS One 16, e0256783. https://doi.org/10.1371/journal.pone.0256783.

Corti, A., Colombo, M., Migliavacca, F., Rodriguez Matas, J.F., Casarin, S., Chiastra, C., 2021. Multiscale computational modeling of vascular adaptation: a systems biology approach using agent-based models. Front. Bioeng. Biotechnol. 9, 744560. https://doi.org/10.3389/fbioe.2021.744560.

Corti, A., Colombo, M., Migliavacca, F., Berceli, S.A., Casarin, S., Rodriguez Matas, J.F., Chiastra, C., 2022a. Multiscale agent-based modeling of restenosis after percutaneous transluminal angioplasty: Effects of tissue damage and hemodynamics on cellular activity. Comput. Biol. Med. 147, 105753. https://doi.org/10.1016/j.compbiomed.2022.105753.

Corti, A., Colombo, M., Rozowsky, J.M., Casarin, S., He, Y., Carbonaro, D., Migliavacca, F., Rodriguez Matas, J.F., Berceli, S.A., Chiastra, C., 2022b. A predictive multiscale model of in-stent restenosis in femoral arteries: linking haemodynamics and gene expression with an agent-based model of cellular dynamics. J. R. Soc. Interface 19, 20210871. https://doi.org/10.1098/rsif.2021.0871.

Corti, A., McQueen, A., Migliavacca, F., Chiastra, C., McGinty, S., 2023a. Investigating the effect of drug release on in-stent restenosis: A hybrid continuum - agent-based modelling approach. Comput. Methods Programs Biomed. 241, 107739. https://doi.org/10.1016/j.cmpb.2023.107739.

Corti, A., Migliavacca, F., Berceli, S.A., Chiastra, C., 2023b. Predicting 1-year in-stent restenosis in superficial femoral arteries through multiscale computational modelling. J. R. Soc. Interface 20, 20220876. https://doi.org/10.1098/rsif.2022.0876.

Corti, A., Marradi, M., Çelikbudak Orhon, C., Boccafoschi, F., Büchler, P., Rodriguez Matas, J.F., Chiastra, C., 2024. Impact of Tissue Damage and Hemodynamics on Restenosis Following Percutaneous Transluminal Angioplasty: A Patient-Specific Multiscale Model. Ann. Biomed. Eng. https://doi.org/10.1007/s10439-024-03520-1.

Edelman, E.R., Rogers, C., 1998. Pathobiologic responses to stenting. Am. J. Cardiol. 81, 4E–6E. https://doi.org/10.1016/s0002-9149(98)00189-1.

Escuer, J., Aznar, I., McCormick, C., Peña, E., McGinty, S., Martínez, M.A., 2021. Influence of vessel curvature and plaque composition on drug transport in the arterial wall following drug-eluting stent implantation. Biomech. Model. Mechanobiol. 20 (2), 767–786. https://doi.org/10.1007/s10237-020-01415-3.

Escuer, J., Schmidt, A.F., Peña, E., Martínez, M.A., McGinty, S., 2022. Mathematical modelling of endovascular drug delivery: Balloons versus stents. Int. J. Pharm. 620, 121742. https://doi.org/10.1016/j.ijpharm.2022.121742.

GBD 2017 Causes of Death Collaborators, 2018. Global, regional, and national age-sex-specific mortality for 282 causes of death in 195 countries and territories, 1980–2017: a systematic analysis for the Global Burden of Disease Study 2017. Lancet 392, 1736–1788. https://doi.org/10.1016/S0140-6736(18)32203-7.

Gijsen, F.J.H., Vis, B., Barrett, H.E., Zadpoor, A.A., Verhagen, H.J., Bos, D., van der Steen, A.F.W., Akyildiz, A.C., 2021. Morphometric and Mechanical Analyses of Calcifications and Fibrous Plaque Tissue in Carotid Arteries for Plaque Rupture Risk Assessment. IEEE Trans. Biomed. Eng. 68, 1429–1438. https://doi.org/10.1109/TBME.2020.3038038.

Guvenir Torun, S., Torun, H.M., Hansen, H.H.G., Gandini, G., Berselli, I., Codazzi, V., de Korte, C.L., van der Steen, A.F.W., Migliavacca, F., Chiastra, C., Akyildiz, A.C., 2021. Multicomponent Mechanical Characterization of Atherosclerotic Human Coronary Arteries: An Experimental and Computational Hybrid Approach. Front. Physiol. 12, 733009. https://doi.org/10.3389/fphys.2021.733009.

Kalkman, D.N., Aquino, M., Claessen, B.E., Baber, U., Guedeney, P., Sorrentino, S., Vogel, B., de Winter, R.J., Sweeny, J., Kovacic, J.C., Shah, S., Vijay, P., Barman, N., Kini, A., Sharma, S., Dangas, G.D., Mehran, R., 2018. Residual inflammatory risk and the impact on clinical outcomes in patients after percutaneous coronary interventions. Eur. Heart J. 39, 4101–4108. https://doi.org/10.1093/eurheartj/ehy633.

Loree, H.M., Grodzinsky, A.J., Park, S.Y., Gibson, L.J., Lee, R.T., 1994. Static circumferential tangential modulus of human atherosclerotic tissue. J. Biomech. 27, 195–204. https://doi.org/10.1016/0021-9290(94)90209-7.

Mandal, P.K., Sarifuddin, Kolachalama, V.B., 2016. Computational model of drug-coated balloon delivery in a patient-specific arterial vessel with heterogeneous tissue composition. Cardiovasc. Eng. Technol. 7, 406–419. https://doi.org/10.1007/s13239-016-0273-y.

McGinty, S., 2014. A decade of modelling drug release from arterial stents. Math. Biosci. 257, 80–90. https://doi.org/10.1016/j.mbs.2014.06.016.

McQueen, A., Escuer, J., Aggarwal, A., Kennedy, S., McCormick, C., Oldroyd, K., McGinty, S., 2021. Do we really understand how drug eluted from stents modulates arterial healing? Int. J. Pharm. 601, 120575. https://doi.org/10.1016/j.ijpharm.2021.120575.

McQueen, A., Escuer, J., Schmidt, A.F., Aggarwal, A., Kennedy, S., McCormick, C., Oldroyd, K., McGinty, S., 2022. An intricate interplay between stent drug dose and release rate dictates arterial restenosis. J. Control. release Off. J. Control. Release Soc. 349, 992–1008. https://doi.org/10.1016/j.jconrel.2022.07.037.

Milzi, A., Lemma, E.D., Dettori, R., Burgmaier, K., Marx, N., Reith, S., Burgmaier, M., 2021. Coronary plaque composition influences biomechanical stress and predicts plaque rupture in a morpho-mechanic OCT analysis. Elife 10. https://doi.org/10.7554/eLife.64020.

Mukheja, Y., Sarkar, A., Arora, R., Pal, K., Ahuja, A., Vashishth, A., Kuhad, A., Chopra, K., Jain, M., 2024. Unravelling the progress and potential of drug-eluting stents and drug-coated balloons in cardiological insurgencies. Life Sci. 352, 122908. https://doi.org/10.1016/j.lfs.2024.122908.

Nolan, D.R., Lally, C., 2018. An investigation of damage mechanisms in mechanobiological models of in-stent restenosis. J. Comput. Sci. 24, 132–142. https://doi.org/10.1016/j.jocs.2017.04.009.

Sarifuddin, Mandal, P.K., 2024. Plaque heterogeneity and the spatial distributions of its components dictate drug-coated balloon therapy. Sci. Rep. 14, 4412. https://doi.org/10.1038/s41598-024-54756-9.

Schillinger, M., Exner, M., Mlekusch, W., Haumer, M., Ahmadi, R., Rumpold, H., Wagner, O., Minar, E., 2002a. Balloon angioplasty and stent implantation induce a vascular inflammatory reaction. J. Endovasc. Ther. 9, 59–66. https://doi.org/10.1177/152660280200900111.

Schillinger, M., Exner, M., Mlekusch, W., Rumpold, H., Ahmadi, R., Sabeti, S., Haumer, M., Wagner, O., Minar, E., 2002b. Vascular inflammation and percutaneous transluminal angioplasty of the femoropopliteal artery: association with restenosis. Radiology 225, 21–26. https://doi.org/10.1148/radiol.2251011809.

Serafini, E., Corti, A., Gallo, D., Chiastra, C., Li, X.C., Casarin, S., 2023. An agent-based model of cardiac allograft vasculopathy: toward a better understanding of chronic rejection dynamics. Front. Bioeng. Biotechnol. 11, 1190409. https://doi.org/10.3389/fbioe.2023.1190409.

Shlofmitz, E., Iantorno, M., Waksman, R., 2019. Restenosis of Drug-Eluting Stents: A New Classification System Based on Disease Mechanism to Guide Treatment and State-of-the-Art Review. Circ. Cardiovasc. Interv. 12, e007023. https://doi.org/10.1161/CIRCINTERVENTIONS.118.007023.

Stefanati, M., Corti, A., Corino, V.D.A., Bennett, M.R., Teng, Z., Dubini, G., Rodriguez Matas, J.F., 2024. Effect of variability of mechanical properties on the predictive capabilities of vulnerable coronary plaques. Comput. Methods Programs Biomed. 254, 108271. https://doi.org/10.1016/j.cmpb.2024.108271.

Tahir, H., Hoekstra, A.G., Lorenz, E., Lawford, P.V., Hose, D.R., Gunn, J., Evans, D.J.W., 2011. Multi-scale simulations of the dynamics of in-stent restenosis: impact of stent deployment and design. Interface Focus 1, 365–373. https://doi.org/10.1098/rsfs.2010.0024.

Tahir, H., Bona-Casas, C., Hoekstra, A.G., 2013. Modelling the effect of a functional endothelium on the development of in-stent restenosis. PLoS One 8, e66138. https://doi.org/10.1371/journal.pone.0066138.

Tahir, H., Niculescu, I., Bona-Casas, C., Merks, R.M.H., Hoekstra, A.G., 2015. An in silico study on the role of smooth muscle cell migration in neointimal formation after coronary stenting. J. r. Soc. Interface 12, 20150358. https://doi.org/10.1098/rsif.2015.0358.

Zahedmanesh, H., Van Oosterwyck, H., Lally, C., 2014. A multi-scale mechanobiological model of in-stent restenosis: deciphering the role of matrix metalloproteinase and extracellular matrix changes. Comput. Methods Biomech. Biomed. Engin. 17, 813–828. https://doi.org/10.1080/10255842.2012.716830.

Zun, P.S., Anikina, T., Svitenkov, A., Hoekstra, A.G., 2017. A Comparison of Fully-Coupled 3D In-Stent Restenosis Simulations to In-vivo Data. Front. Physiol. 8, 284. https://doi.org/10.3389/fphys.2017.00284.

Zun, P.S., Narracott, A.J., Chiastra, C., Gunn, J., Hoekstra, A.G., 2019. Location-specific comparison between a 3D in-stent restenosis model and micro-CT and histology data from porcine in vivo experiments. Cardiovasc. Eng. Technol. 10, 568–582. https://doi.org/10.1007/s13239-019-00431-4.